Power Electronics and Drives
Volume 11(46), 2026 DOI: 10.2478/pead-2026-0007

Power Electronics and Drives

Fault-Tolerant Reconfiguration for Two Cascaded Two-Level Inverters Feeding the Dual Open-End Stator Windings of an Induction Motor

Research Paper

Sami Guizani[1,3], Abdelmonoem Nayli[2,3,*]

[1]*University of EL Manar, IPEIEM, Tunisia, Tunisia.*
[2]*University of Gafsa, IPEIG, Gafsa, Tunisia.*
[3]*University of Carthage, MMA Laboratory, INSAT, Tunisia, Tunisia*

Received: 22 November, 2025; Received in the revised form: 31 January, 2026; Accepted: 25 February, 2026

Abstract: The primary goal of this work is to significantly enhance the availability and operational reliability of a variable speed drive system, a factor critical for industrial processes where downtime must be minimised. This improvement is rooted in a robust power architecture: a dual open-end stator winding induction machine is utilised, where each entry of the machine is supplied by two cascaded two-level inverters, thereby increasing the system's inherent redundancy. The control strategy employed is the phase disposition pulse width modulation (PD-PWM) technique. The study comprehensively analyses the system's behaviour under various fault configurations, focusing specifically on the failure of a single cascaded inverter and rigorously defines the critical operating and control conditions that must be implemented to maintain system functionality. Simulation results successfully demonstrate the effectiveness of this machine-cascaded inverter association in a degraded operating mode, ensuring continuity of service with rotation speeds very close to the nominal value, thereby validating the robustness of the chosen architecture for high-reliability applications.

Keywords: *dual open-end stator winding induction machine • cascaded two-level inverters • power segmentation • reliability*

1. Introduction

Open-end stator winding AC machines have become a focal point of contemporary research, primarily due to their inherent capacity for power segmentation and their ability to maintain operation in degraded modes (Guizani et al., 2016; Nayli et al., 2025). A standard example is the open-end winding induction machine (OEWIM), typically driven by a dual two-level inverter configuration where each unit is rated for 50% of the nominal power. This topology provides a significant degree of freedom for fault-tolerant operation.

Building upon this concept, the dual open-end stator winding induction machine (DOESWIM) offers even greater flexibility. The DOESWIM architecture consists of two sets of three-phase open-end windings, requiring a drive system equipped with four voltage-source inverters (VSIs). In this configuration, each inverter is dimensioned for a power rating equivalent to 25% ($P/4$) of the machine's total capacity. This association with two-level inverters allows the drive to tolerate up to three successive failures, facilitating operation in both active and passive redundancies (Guizani and Ben Ammar, 2015).

Considerable research has been dedicated to proposing diverse inverter structures for open-end winding machines. These include three-phase two-level inverters using either a single DC link (Somasekhar et al., 2004; Zhi et al., 2025) or independent DC links (Greeshma and Arun Rahul, 2022). Furthermore, multilevel topologies such as neutral-point clamped (NPC) (Ehsan and Farhad, 2022; Supratik et al., 2021), flying capacitor (FC)

* *Email: abdelmonoem.nayli@gmail.com*

(Boris et al., 2019), and various hybrid inverter types (Kasinath et al., 2021; Parimalasundar et al., 2023; Xiaogang et al., 2024) have been explored. Specifically, the use of two cascaded two-level inverters has been shown to enhance the drive's dependability, increase voltage levels, and improve both current quality and torque stability (Guizani and Ben Ammar, 2018).

In this context, this paper examines the association of a DOESWIM with a redundant power system comprising two cascaded two-level inverters per winding set to ensure service continuity during fault conditions. The first section establishes the simulation model of the DOESWIM supplied by a total of four converter units. The second section focuses on the performance analysis of the machine under post-fault operation. This includes the detailed investigation of four specific fault configurations and the rigorous definition of control strategies required to preserve the system's functional integrity.

2. Supply of the DOESWIM by Two Cascaded Two-Level Inverters

Figure 1a presents the configuration of the DOESWIM, which is fed by four separate converters. The converter topology, illustrated in Figure 1b, comprises two cascaded two-level inverters. A V/f control scheme is implemented to manage the fundamental operation.

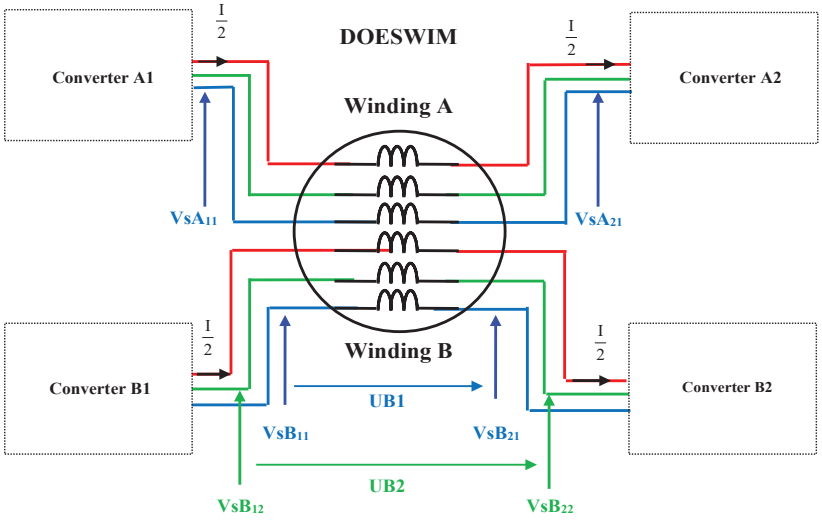

(a)

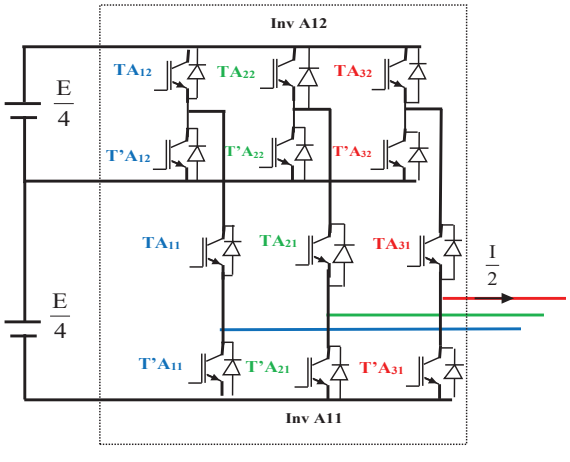

(b)

Figure 1. (a) DOESWIM supplied by two cascaded two-level inverters. (b) Structure of the two cascaded two-level inverters.

The drive system is controlled via phase disposition pulse width modulation (PD-PWM). This technique compares three 120°-shifted reference voltages (frequency, f_s) with two triangular carriers (frequency, f_p = 5 kHz). As illustrated in Figure 2, this logic drives the cascaded inverters for input A1 (stator A) and B1 (stator B). To implement the open-end winding configuration, a second set of references, shifted by 180° relative to the first, controls the inverters at inputs A2 and B2.

The variation of the speed, the two-stator currents, and the torques for the two windings A and B of the machine are shown in Figure 3. The operational cycle proceeds as follows: at t = 0.6 s, the system initiates a starting sequence. The machine then runs under no-load conditions from t = 0.6 s to t = 1 s. Subsequently, a load torque (T_r = 300 Nm) is introduced at t = 1 s for the remainder of the cycle.

The variations of the phase-to-phase voltages from converters A_1, A_2, B_1, and B_2, along with the machine voltages U_A (winding A) and U_B (winding B) in steady-state mode, are shown in Figure 4. With different pole voltages:

$$U_{A1} = Vs_{A11} - Vs_{A12} \text{ of converter } A_1 \text{ and } U_{A2} = Vs_{A21} - Vs_{A22} \text{ of converter } A_2$$

$$U_A = U_{A1} - U_{A2} \text{ of winding A and } U_B = U_{B1} - U_{B2} \text{ of winding B.}$$

Table 1 provides a comprehensive comparison of the simulated performance metrics for various inverter topologies used to power the OEWIM and DOESWIM (Guizani and Ben Ammar, 2018; Guizani et al., 2016). Specifically, it contrasts conventional inverters with the two-cascaded inverter configuration. The comparison

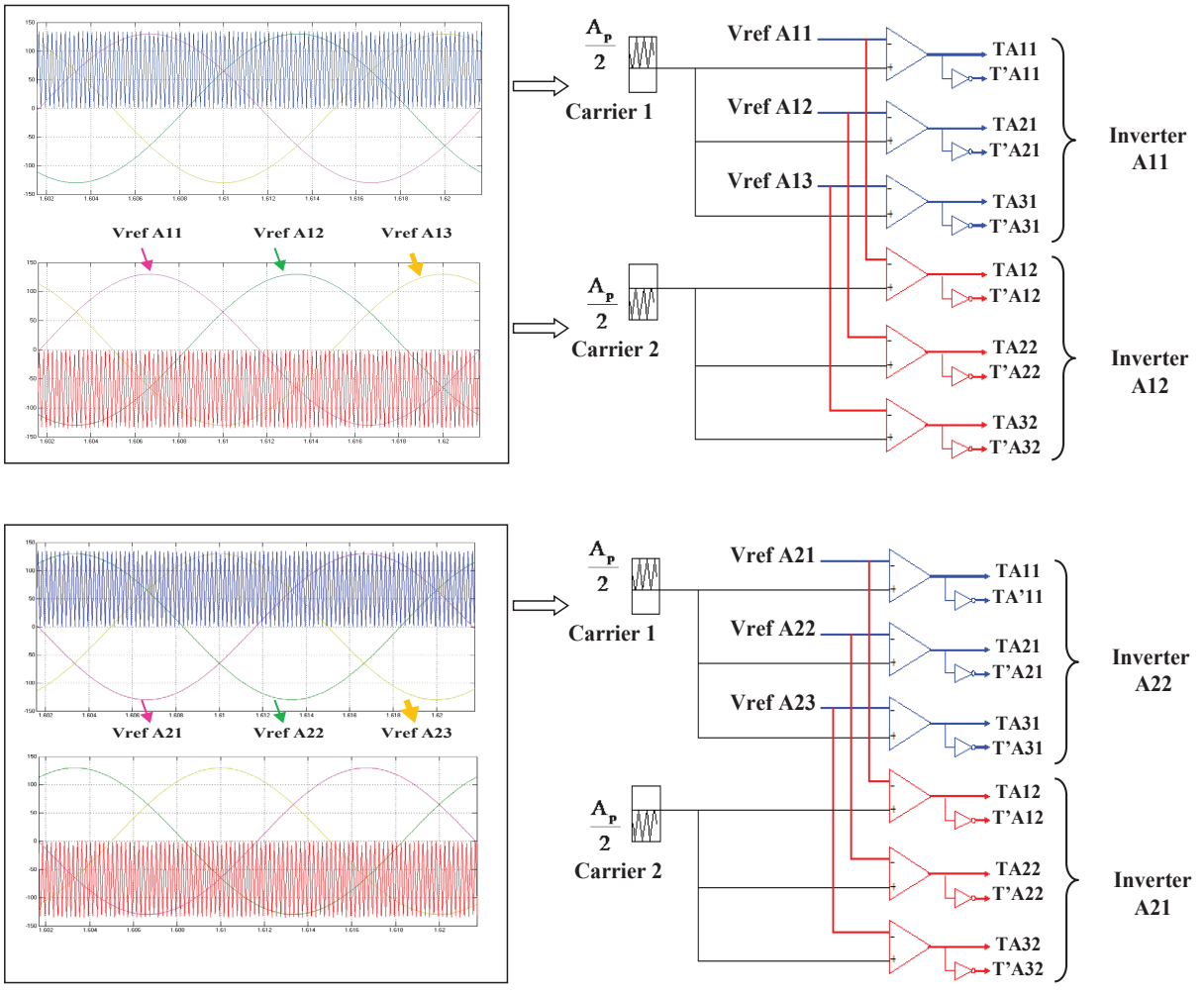

Figure 2. Principle of the phase-disposition PWM for two cascaded inverters. PWM, pulse width modulation.

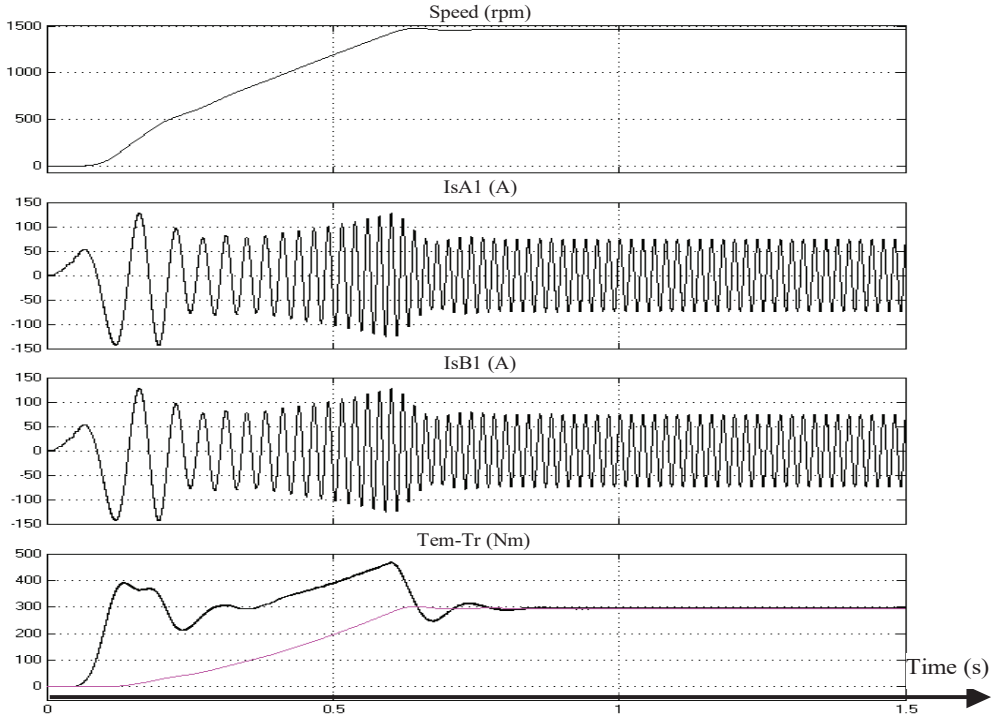

Figure 3. Variation of the speed, the two-stator currents, and the torques.

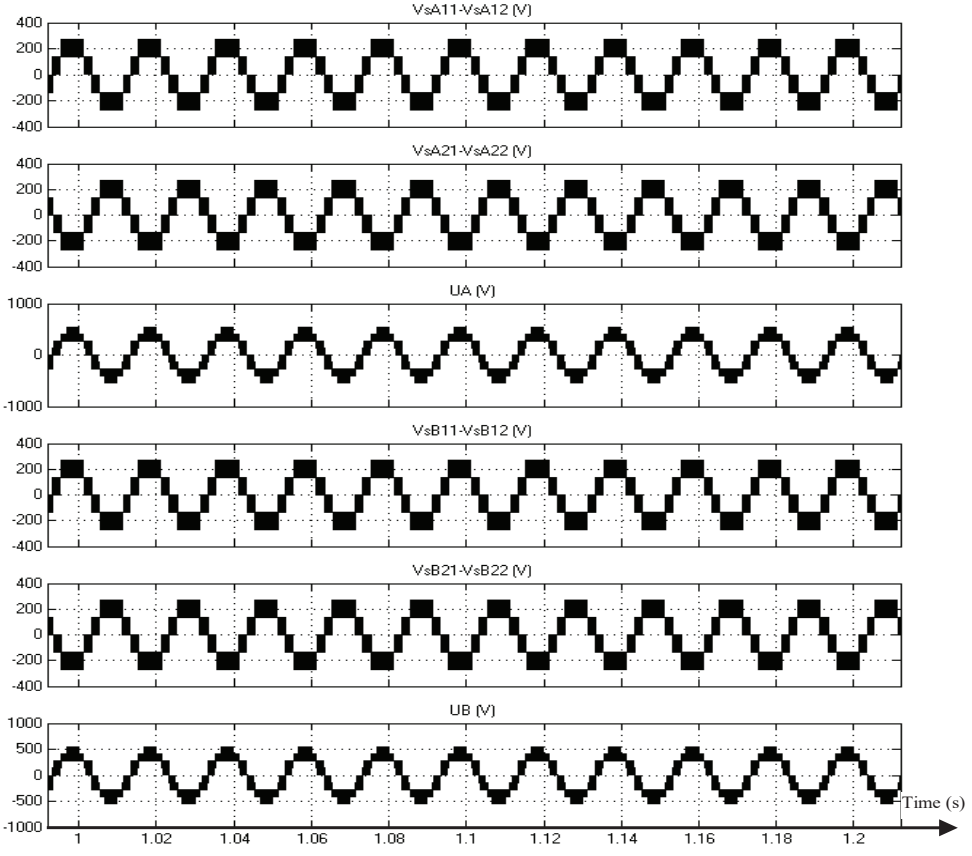

Figure 4. Variation of the pole's voltage converters and machine.

Table 1. Comparative analysis of the proposed architectures.

	OEWIM Two-level inverter	OEWIM Two cascaded Two-level inverters	DOESWIM Two-level inverter	DOESWIM Two cascaded Two-level inverters
Number of voltage level	3	5	3	5
DC voltage value	*E*/2	*E*/4	*E*/2	*E*/4
Sizing of inverter power	*P*/2	Inverter A11: *P*/2 Inverter A12: *P*/4	*P*/4	Inverter A11: *P*/2 Inverter A12: *P*/4
Current *I* (A)	*I*	*I*	*I*/2	*I*/2
THD voltage (%)	44.27	24.99	43.86	26.77
THD current (%)	0.52	0.39	0.66	0.41
ΔT_{em} (%)	1.26	0.88	1.66	0.83

focuses on key parameters, including the number of voltage levels, DC bus voltage requirements, inverter power ratings, the total harmonic distortion (THD) of both voltage and stator current, and the torque ripple characteristics.

The synergistic integration of cascaded inverters with OEWIM and DOESWIM configurations introduces a step-change in drive system performance. By leveraging the staggered switching of the cascaded stages, the phase-to-phase voltage resolution is elevated from a standard three-level to a five-level stepped waveform. This transition to a higher number of levels significantly smoothens the voltage profile, leading to a drastic attenuation of the THD. From a mechanical perspective, this superior spectral quality directly mitigates high-frequency flux pulsations, thereby minimising torque ripple and reducing acoustic noise and mechanical stress. Furthermore, the DOESWIM architecture excels in power segmentation (power splitting), allowing the total machine load to be distributed across multiple independent inverter units. Beyond efficiency, this redundancy inherently bolsters system reliability and availability. By providing extra degrees of freedom, the system can implement fault-tolerant strategies, ensuring continued operation even in the event of a partial inverter failure.

3. Degraded Mode Operation

This section investigates the operation of the DOESWIM driven by two cascaded two-level inverters under a single-inverter failure condition. It is important to emphasise that while a short transient occurs during the fault, the mechanical inertia of the induction motor (IM) acts as a low-pass filter, significantly damping speed oscillations during this brief window. In the case of the DOESWIM, the magnetic coupling between the two sets of windings provides a degree of natural redundancy. During the detection delay, the healthy winding set maintains the rotating magnetic field, which further mitigates the impact on the electromagnetic torque and speed compared to conventional machines.

3.1. Configuration 1

The first configuration corresponds to an open-circuit fault on the power switches T'A12, T'A22, or T'A32 of inverter A22. Consequently, the control sets switches T'A12, T'A22, and T'A32 to state 0 and switches TA12, TA22, and TA32 to state 1, as represented in Figure 5. Given that the DC bus voltage at point A2 equals *E*/2, the machine is capable of operation at its nominal speed. Because inverter A21 is sized for a power rating of *P*/4, no specific operating conditions are necessary.

Figure 6 presents the simulation results for a load torque $T_r = k\omega^2$, detailing the stator currents, speed, and torque. A failure was subsequently simulated in inverter A22 at time $t = 1.2$; this test demonstrated that the system maintained the nominal speed and the machine continued operating seamlessly in normal mode under this fault configuration.

Figure 7 shows the detailed behaviour of the phase-to-phase voltage converters U_{A1} of entry A_1, U_{A2} of entry A_2, U_{B1} of entry B_1, and U_{B2} of entry B_2 in permanent mode. Thus, machine voltage $U_A = U_{A1} - U_{A2}$ of winding A and $U_B = U_{B1} - U_{B2}$ of winding B for the fault of inverter A_{22} at $t = 1.2$ s.

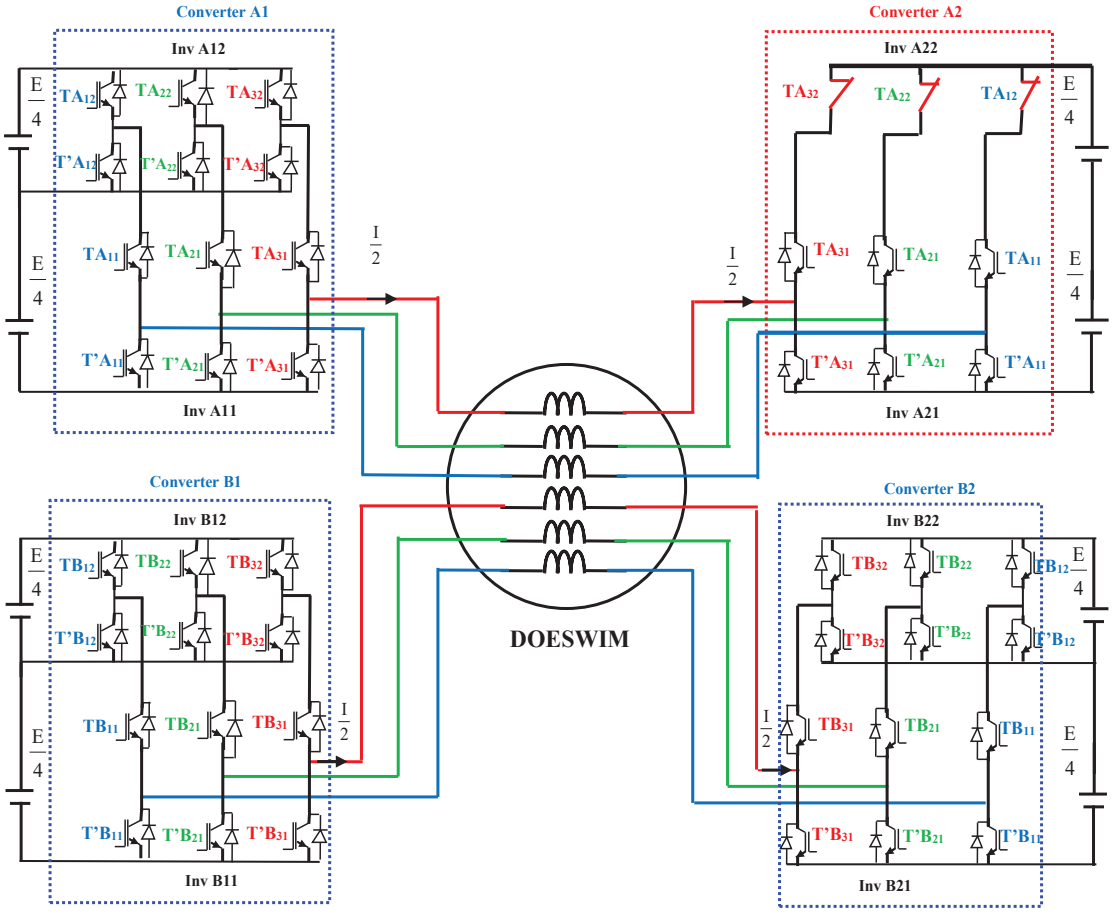

Figure 5. Feeding of DOESWIM by four converters for the first configuration.

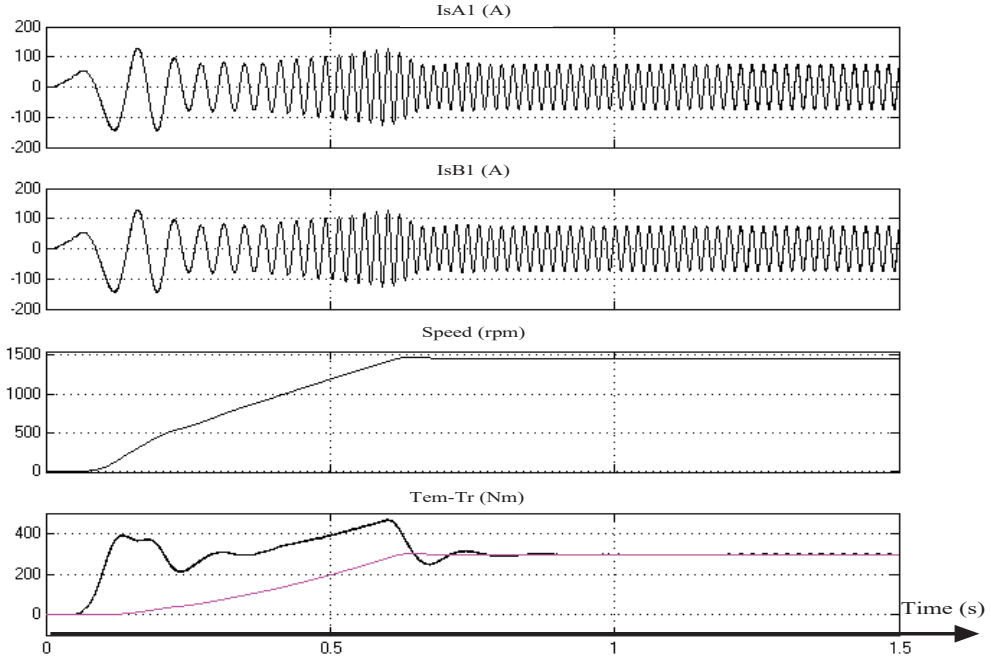

Figure 6. Variation of the two-stator currents, speed, and torques for the first configuration.

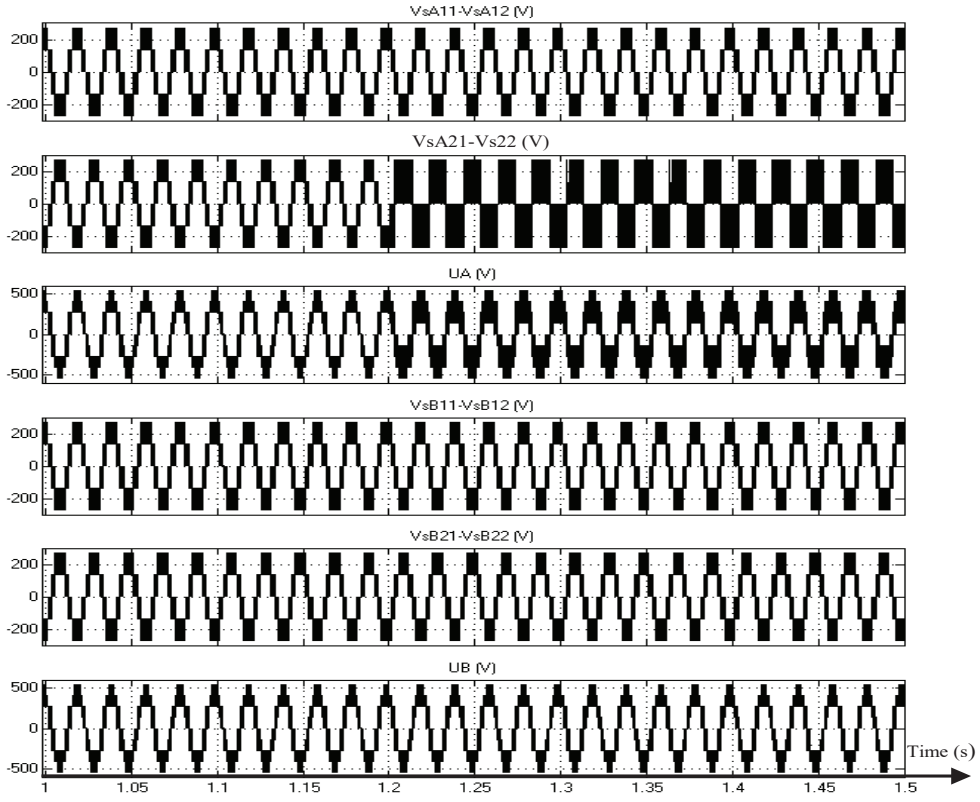

Figure 7. Variation of the phase-to-phase voltage inverters and machine for the first configuration.

3.2. Configuration 2

Considering the second fault mode, depicted in Figure 8a, where an open-circuit fault occurs on one of the power devices (TA12, TA22, or T32) within inverter A22, the supervisory control mandates a specific response: switches TA12, TA22, and TA32 are deactivated (state 0), while their counterparts, T'A12, T'A22, and T'A32, are activated (state 1) (Figure 8b). Furthermore, the machine's A_2 input, fed by inverter A_{21}, requires the DC bus voltage to be precisely $E/4$. This same voltage must also be supplied to input B_2, which draws power from inverter B_{21}, a condition critical for preventing stator winding imbalance between the three-phase windings A and B. As a direct result, and to safeguard against peak currents, the machine's operational limit is reduced to 86% of its nominal speed under the torque characteristic $T_r = k\omega^2$.

Figure 9 shows a magnified view of the pole voltages for the four converters and the phase-to-phase machine voltage, highlighting the behaviour before and after the failure of inverter A22 in steady-state operation. At time $t = 1.2$ s, there will be a failure by inverter A22, therefore a supply by inverter A21 of the winding A and the inverter B21 of the winding B with continuous bus voltage $E/4$ of each entry A2 and B2.

The simulation results of the two-stator currents, speed, and torque for the machine operation in degraded mode is shown in Figure 10. Also, at time $t = 1.2$ s, the speed reduces 86% of its nominal value for a load torque $T_r = k\omega^2$.

3.3. Configuration 3

The third fault mode, which is depicted in Figure 11a, is defined by an open-circuit failure on one of the power devices (T'A11, T'A21, or T'A31) within inverter A21. In response to this event, the supervisory control system implements a precise strategy: the faulty switches (T'A11, T'A21, and T'A31) are commanded to state 0 (deactivated), while their complementary devices (TA11, TA21, and TA31) are set to state 1 (activated) (Figure 11b). Regarding the machine's power supply, the A2 input, which is fed by inverter A22, requires the DC bus voltage to be precisely $E/4$. Critically, this same voltage must be applied to input B2, which draws power from inverter B22, as this equality is essential to prevent stator winding imbalance between the three-phase windings A and B. Consequently, and with the objective of mitigating current peaks, the operational limit of the machine is restricted to 86% of its nominal

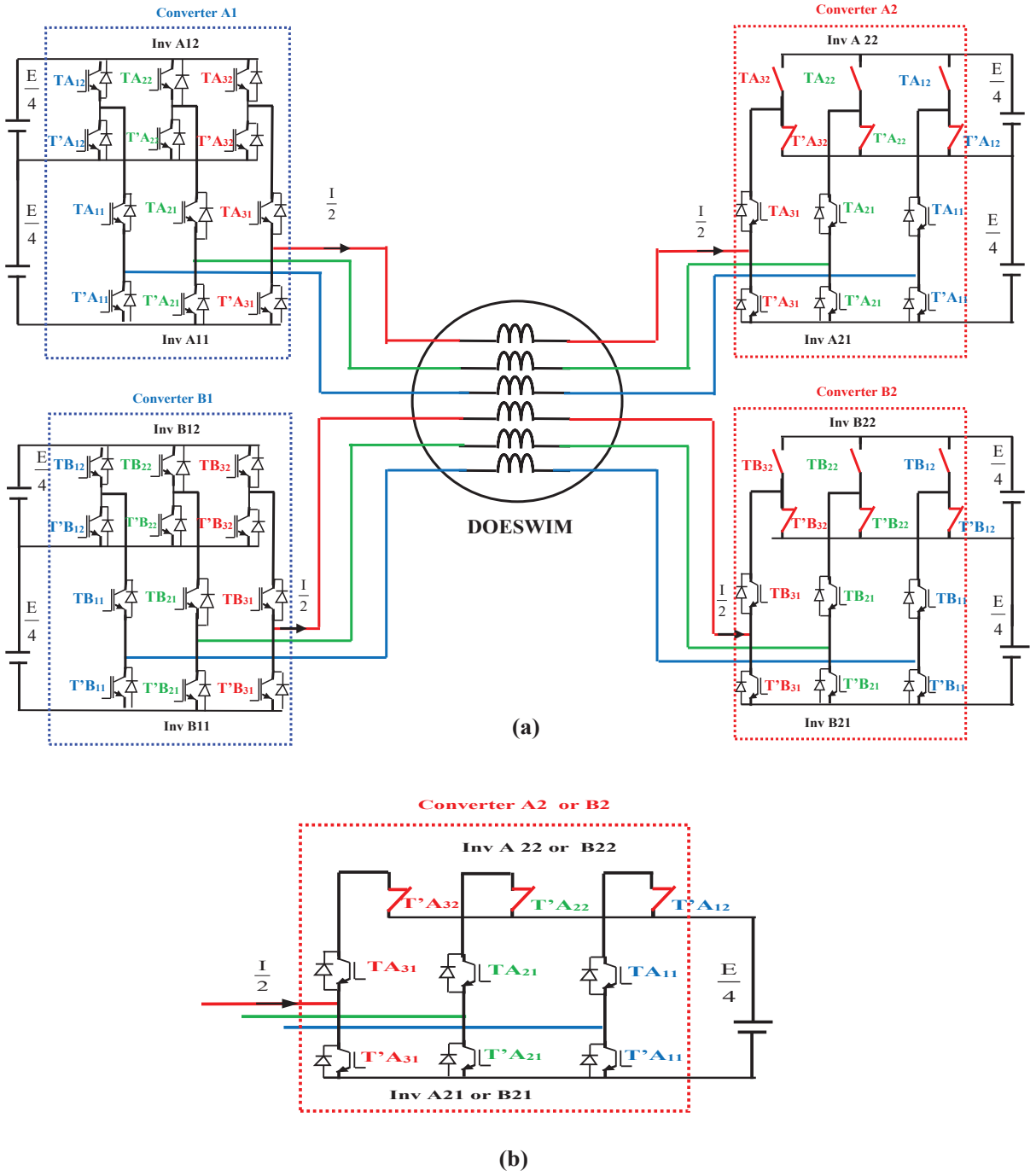

Figure 8. (a) Feeding of the DOESWIM by four converters for the second configuration. (b) Reconfiguration of the converters A2 and B2 for the second configuration.

speed under the prescribed torque characteristic $T_r = k\omega^2$. The results obtained from this configuration are consistent with those of the previous configuration (also illustrated) and serve to validate the effectiveness of this control strategy.

Figure 12 shows the same simulation results than the second configuration of the pole voltage of the four converters and phase-to-phase machine voltage before and after the failure of inverter A21 and inverter B21.

The simulation results of the two-stator current, speed, and torque reducing 86% of its nominal value for a load torque $T_r = k\omega^2$ is shown in Figure 13.

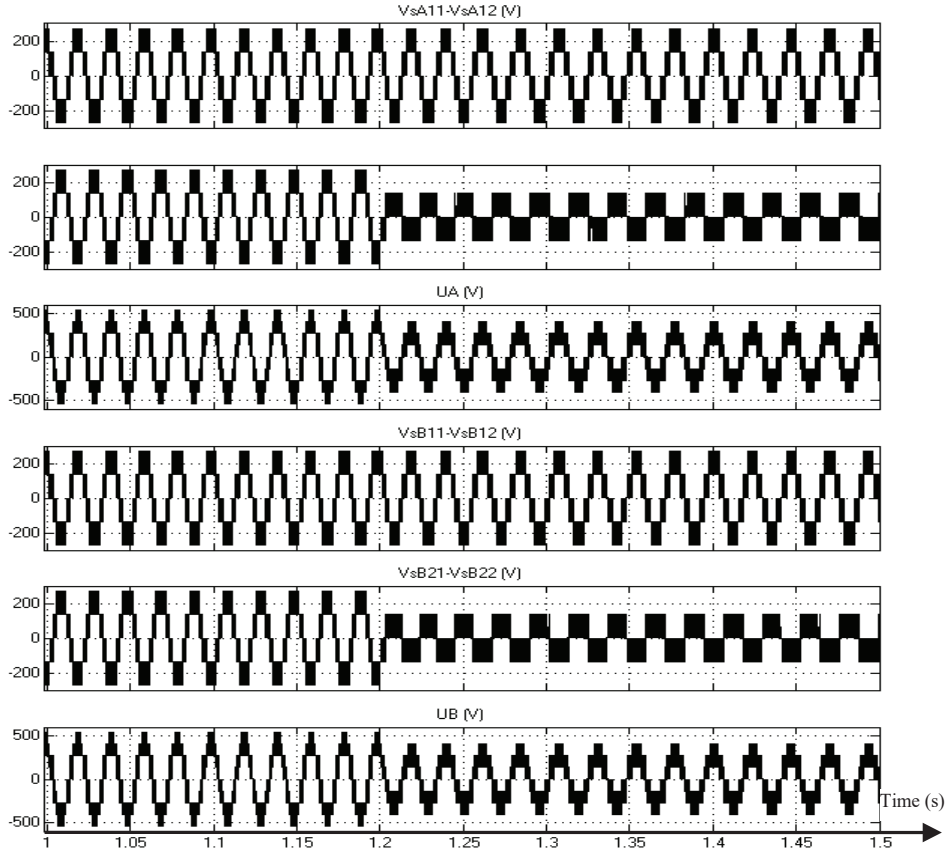

Figure 9. Variation of the phase-to-phase voltage inverters and machine for the second configuration.

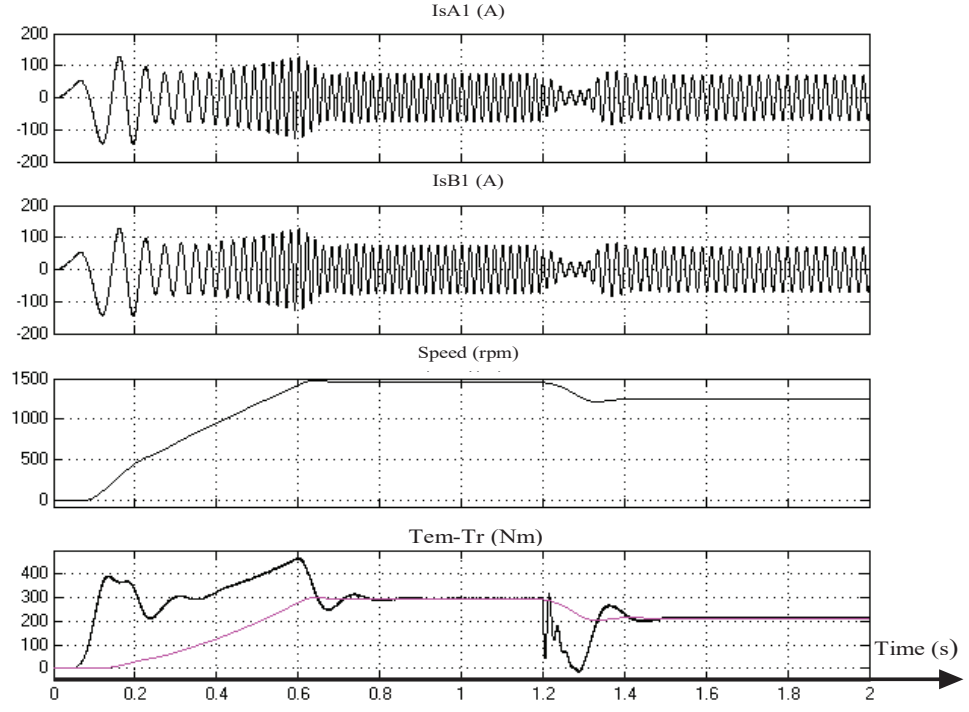

Figure 10. Variation of the two-stator currents, speed, and torque for the second configuration.

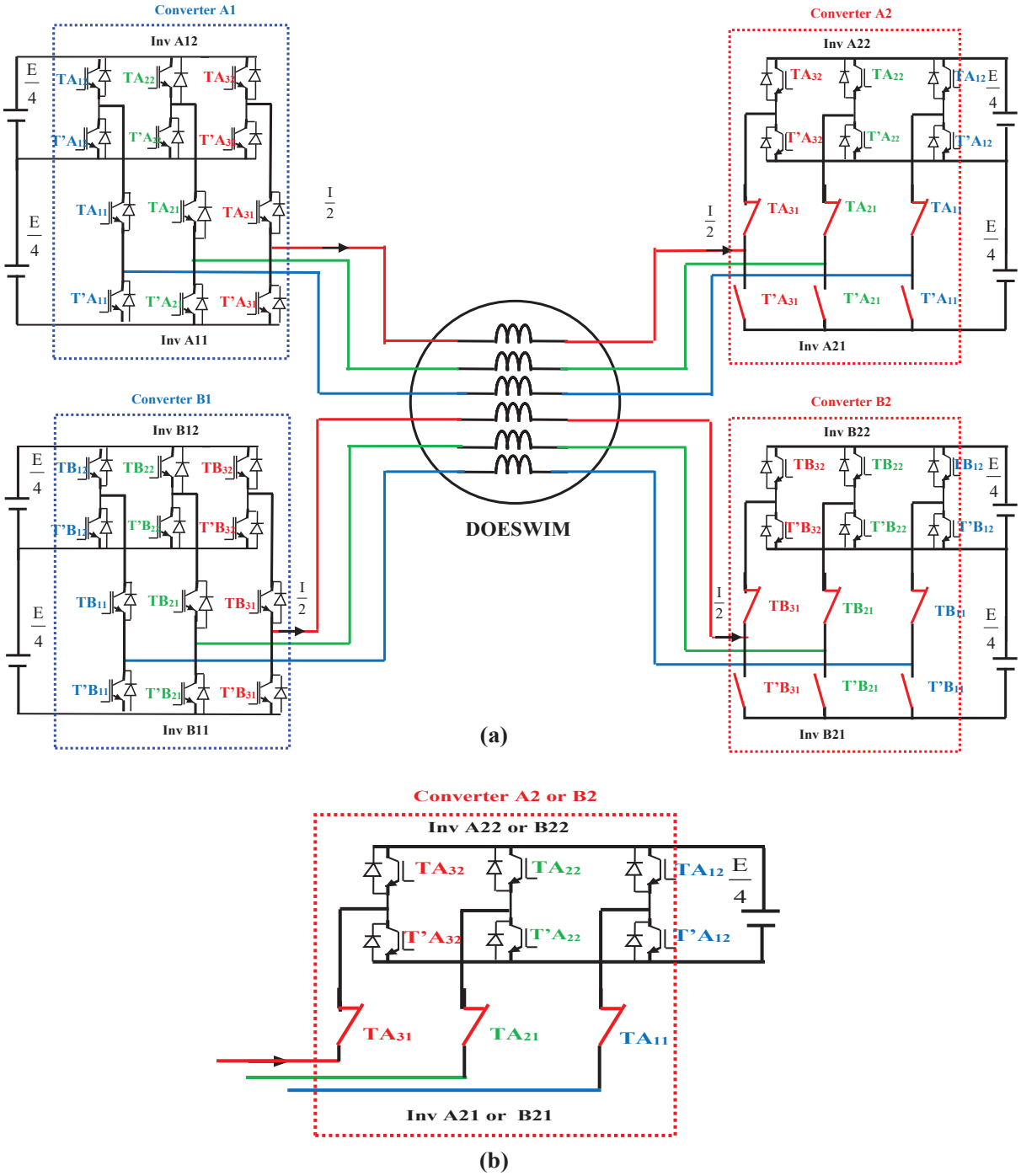

Figure 11. (a) Feeding of the DOESWIM by four converters for the third configuration. (b) Reconfiguration of the converters A2 and B2 for the third configuration.

3.4. Configuration 4

The fourth configuration, which is depicted in Figure 14, involves an open-circuit fault on one of the power switches (TA11, TA21, or TA31) of inverter A11. In response to this failure, the supervisory control system must intervene by blocking (state 0) the three switches TA11, TA21, and TA31 and simultaneously turning ON (state 1) their

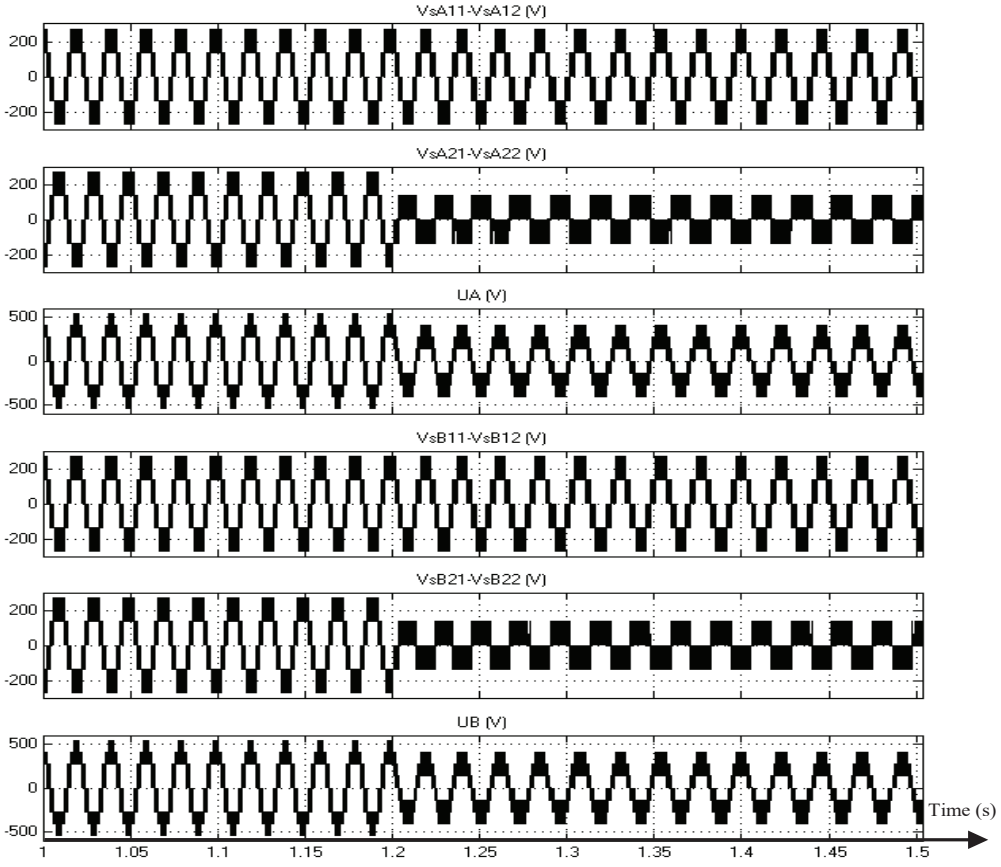

Figure 12. Variation of the phase-to-phase voltage inverters and machine for the third configuration.

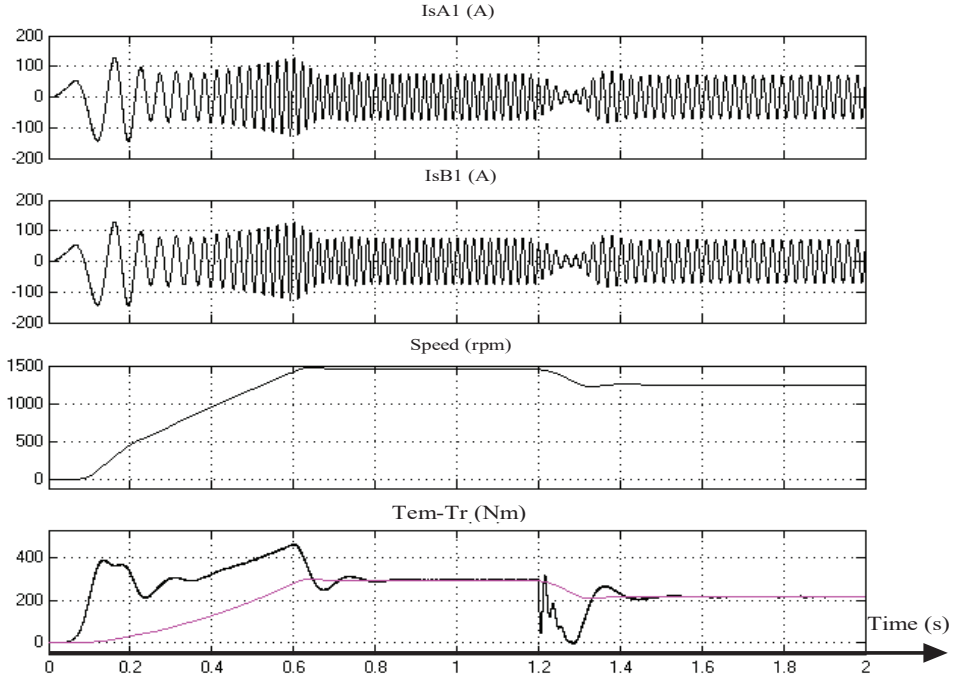

Figure 13. Variation of the two-stator currents, speed, and torque for the third configuration.

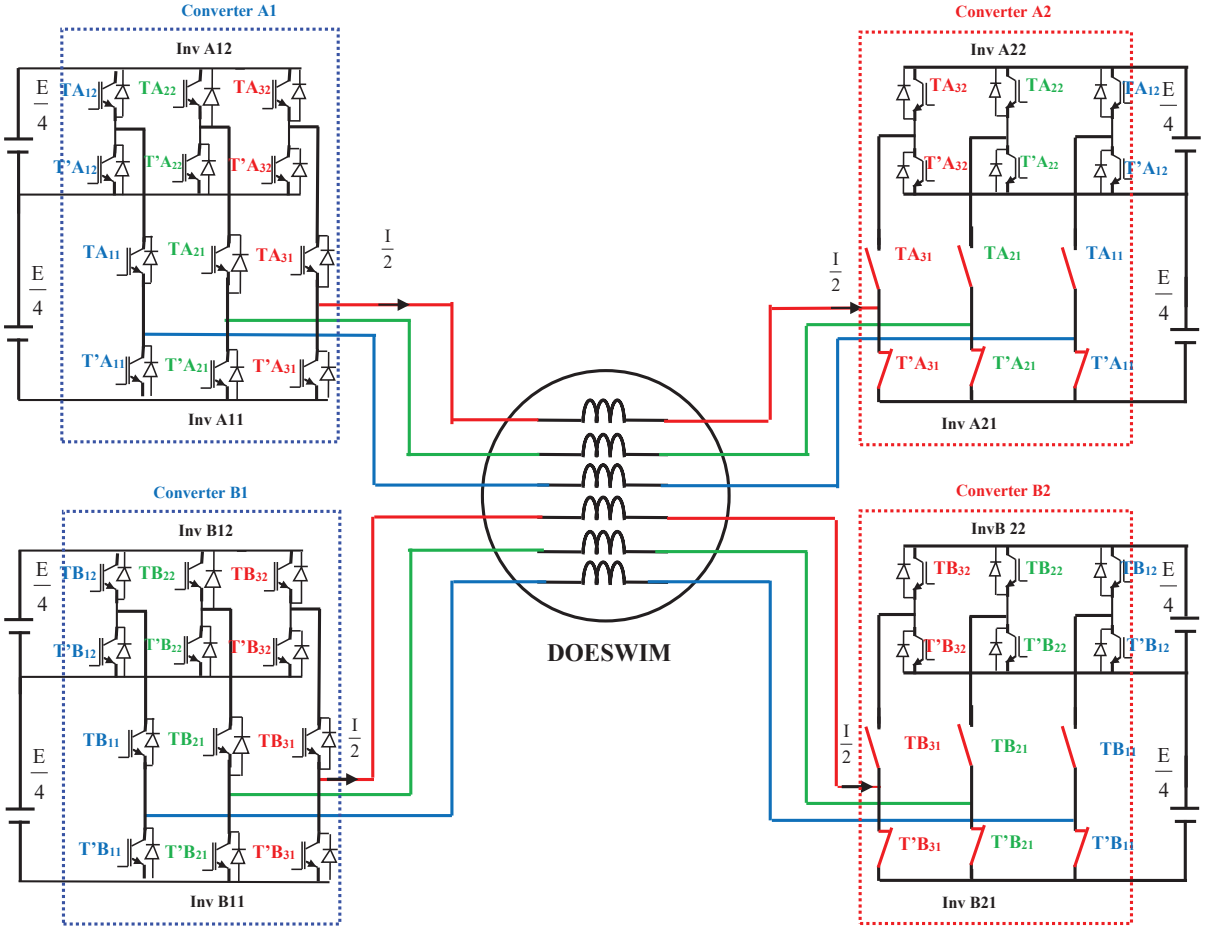

Figure 14. Feeding of the DOESWIM by four converters for the fourth configuration.

complementary switches, T'A11, T'A21, and T'A31. An identical reconfiguration must be applied to the control switches of inverter B11 to avoid imbalance of the stator windings A and B. This strategy results in a star coupling (or Y-coupling) of the machine's A and B input windings, corresponding to the operational mode of the double-star asynchronous machine powered by two converters. The post-fault state mandates that the machine operates at a reduced speed, specifically 70% of the nominal speed, under the load torque $T_r = k\omega^2$. Consequently, since the operational constraints are significantly reduced compared to the nominal regimen, no additional conditions are imposed on the initial sizing of the inverters to maintain this performance level.

This strategy results in a star coupling (or Y-coupling) of the machine's A and B input windings, corresponding to the operational mode of the double-star asynchronous machine powered by two converters, as shown in Figure 15. The post-fault state mandates that the machine operates at a reduced speed, specifically 70% of the nominal speed, under the load torque $T_r = k\omega^2$. Consequently, since the operational constraints are significantly reduced compared to the nominal regimen, no additional conditions are imposed on the initial sizing of the inverters to maintain this performance level.

Figure 16 represents the voltage-boosting effect visible in the pole voltages of the four converters and the machine phase-to-phase voltage, both before and after the fault in inverter A21. The fault is simulated at time t = 1.2 s, triggering the intentional deactivation of the inverters connected to terminals A2 and B2. By applying a control reconfiguration strategy, the machine is maintained in operation, albeit with a resulting speed reduction of 70% from the nominal value.

Figure 17 shows the different variations of the two-stator currents, speed, and the torques with reduced speed to 70% of nominal value for a load torque $T_r = k\omega^2$.

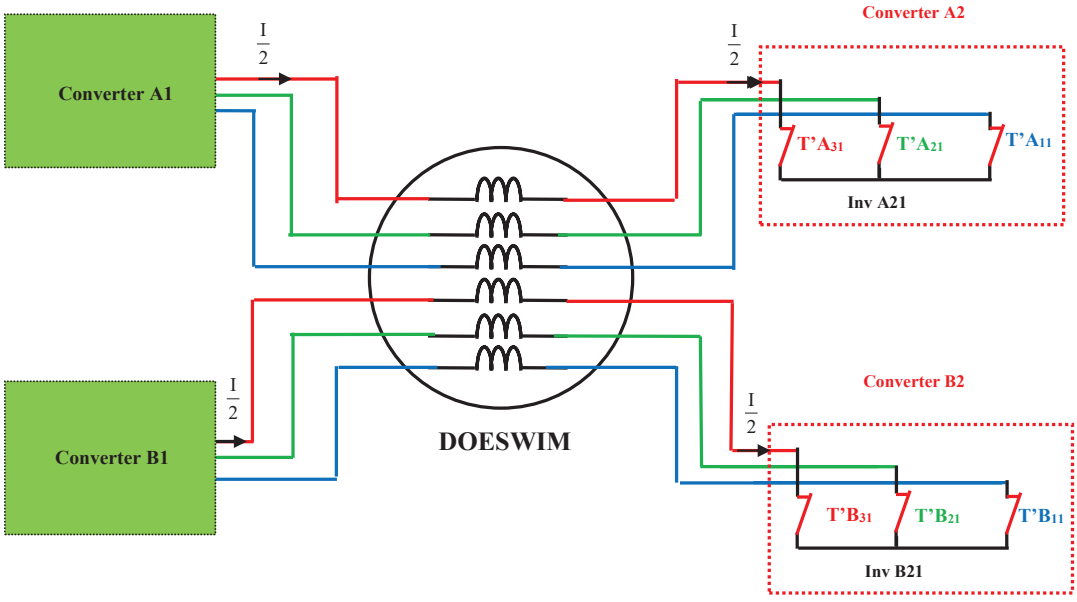

Figure 15. Operational mode of the double star asynchronous machine powered by two converters for the fourth configuration.

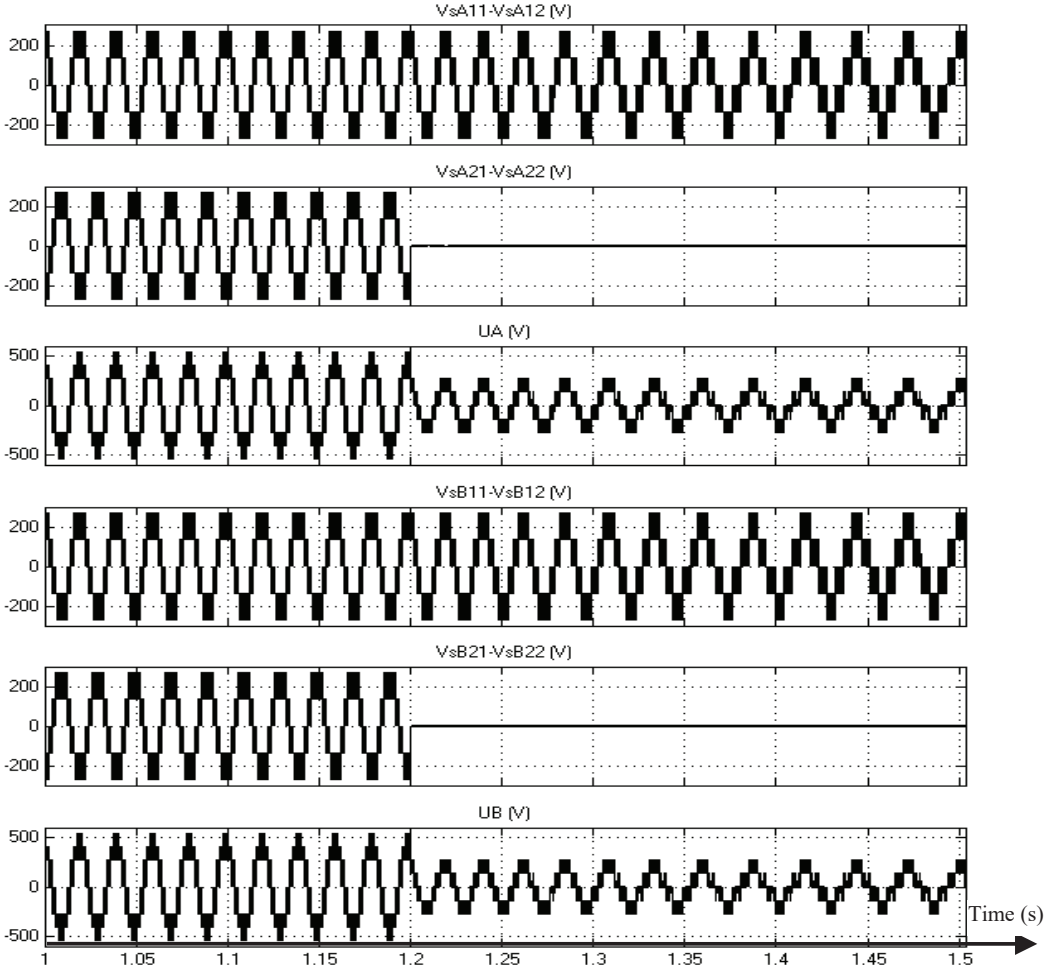

Figure 16. Variation of the phase-to-phase voltage inverters and machine for the fourth configuration.

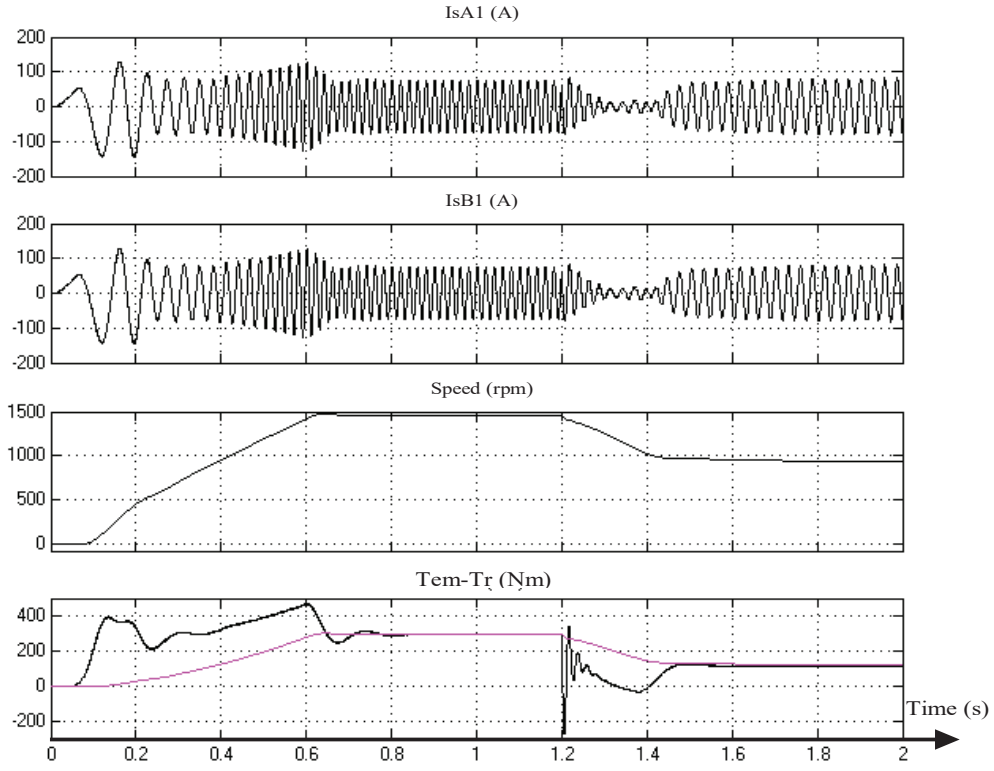

Figure 17. Variation of the two-stator currents, speed, and torque for the fourth configuration.

Table 2. Quantitative performance comparison.

	Nominal Mode	Fault 1	Fault 2	Fault 3	Fault 4
THD current (%)	0.4	2.02	21.5	20.6	32
Torque ripple (%)	0.83	1.3	1.2	0.9	1.2
Peak current (A)	76	76	70	72	76
THD voltage (%)	26.7	40	46.8	42.2	60

It can be observed that the proposed strategy effectively maintains a very low torque ripple (remaining below 1.3% across all cases), which is crucial for the mechanical integrity of the motor. While the THD of the current and voltage increases during degraded operation modes reaching 32% and 60%, respectively, in the most severe case (Fault 4), the system successfully maintains operation and speed stability, which is the primary objective of the fault-tolerant control. Furthermore, the peak current remains within safe limits (around 76 A), ensuring no overcurrent stress on the healthy semiconductor switches. Table 2 summarises the parameters for the normal mode and the four fault cases.

Regarding the harmonic analysis, Figure 18 illustrates the output voltage FFT spectrum for the normal mode, while Figure 19 presents the spectra for fault configurations 1–4. The results demonstrate that despite the fault, the primary harmonic clusters remain centred around the carrier frequency multiples. This spectral distribution explains why the torque ripple remains low even when the total THD increases, as the high-frequency components are naturally filtered by the stator inductance.

The primary parameters of the machine utilised in this study are listed below. The nominal power (P) is 45 kW, with a corresponding nominal speed (n) of 1450 rpm. The electrical parameters are Stator resistance R_s = 0.3 Ω, rotor resistance R_r = 0.046 Ω, stator inductance L_s = 17.9 mH, and rotor inductance L_r = 18.6 mH. The mutual inductances are $M_{srA} = M_{srB} = M_{ss}$ = 17.2 mH.

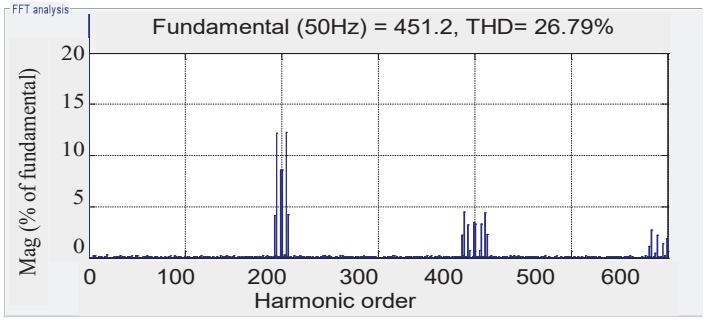

Figure 18. FFT spectra of the output voltage for the normal mode.

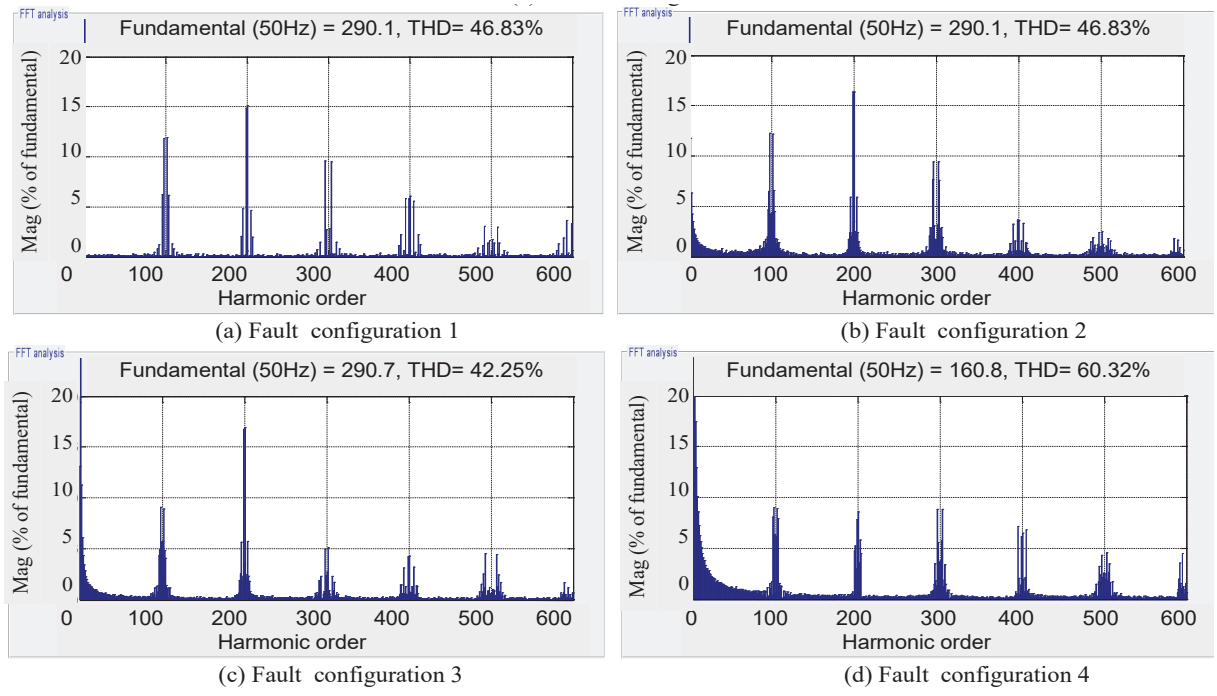

Figure 19. FFT spectra of the output voltage for the different fault configurations.

4. Conclusion

This study demonstrates that the integration of a DOESWIM with two cascaded two-level inverter drives ensures robust operation under degraded modes. The investigation focused on single-inverter failures within the four-stage power system, considering a quadratic load torque characteristic ($T_r = k\omega^2$).

The results identify four distinct fault configurations, all of which guarantee service continuity. The post-fault performance levels are highly favourable:

- Configuration 1 allows the machine to maintain its full nominal speed.
- Configurations 2 and 3 retain significant operational capacity with a coordinated speed reduction to 86% of the rated value.
- Configuration 4 sustains a substantial speed of 70% of the nominal value.

The high degree of performance retention across all studied failure modes confirms that the association between the DOESWIM and cascaded inverters significantly enhances the overall reliability and dependability of the drive system.

Future research will focus on expanding this modular architecture to investigate both healthy- and multi-fault-operating conditions. Key objectives include the mitigation of zero-sequence-circulating currents inherent in open-ended configurations and a comprehensive assessment of real-time computational complexity. Furthermore, experimental validation will be conducted to integrate intelligent fault-tolerant strategies, such as neural networks or fuzzy logic-based observers, to further optimise system resilience.

References

Boris, R., Alexander, R. and Valentina, G. (2019). Analysis of Transients in a Three-Level DC–DC Flying Capacitor Converter. Time Domain Approach. *Power Electronics and Drives*, 4(39), pp. 33–45. doi: 10.2478/pead-2019-0008

Ehsan, A. and Farhad, Z. (2022). Modified Topology and Modulation Technique for Z-Source Neutral-Point Clamped Inverter. *Power Electronics and Drives*, 7(42), pp. 210–226. doi: 10.2478/pead-2022-0016

Greeshma, N. and Arun Rahul, S. (2022). Clamping Modulation Scheme for Low-Speed Operation of Three-Level Inverter Fed Induction Motor Drive with Reduced CMV. *IEEE Transactions on Industry Applications*, 58(6), pp. 7336–7345. doi: 10.1109/TIA.2022.3199193

Guizani, S. and Ben Ammar, F. (2015). Dual Open-End Stator Winding Induction Machine Fed by Redundant Voltage Source Inverters. *Turkish Journal of Electrical Engineering & Computer Sciences*, 23, pp. 2171–2181. doi: 10.3906/elk-1305-80

Guizani, S. and Ben Ammar, F. (2018). Torque and Current Enhancement Based on Dual Open-End Stator Winding IM at 0° Fed by Two 2-Level Cascaded Inverters. *Electrical Engineering*, 3, pp. 1869–1879. doi: 10.1007/s00202-017-0668-2

Guizani, S., Nayli, A. and Ben Ammar, F. (2016). Comparison Between Star Winding and Open-End Winding Induction Machines. *Electrical Engineering*, 98, pp. 219–232. doi: 10.1007/s00202-016-0359-4

Kasinath, J., Chinmoy, K. P.i and Krishna, K. G. (2021). A New 13-Level Switched-Capacitor Inverter With Reduced Device Count. *Power Electronics and Drives*, 6(41), pp. 26–41. doi: 10.2478/pead-2021-0005

Nayli, A., Guizani, S. and Ben Ammar, F. (2025). Experimental Analysis for Star and Open-End Stator Winding Structures of IM. *Power Electronics and Drives*, 10, pp. 271–286. doi: 10.2478/pead-2025-0019

Parimalasundar, E., Muthukaruppasamy, S., Dharmaprakash, R. and Suresh, K. (2023). Performance Investigations of Five-Level Reduced Switches Count H-Bridge Multilevel Inverter. *Electrical Engineering & Electromechanics*, 6, pp. 58–62. doi: 10.20998/2074-272X.2023.6.10

Somasekhar, V. T., Baiju, M. R. and Gopakumar, K. (2004). Dual Two-Level Inverter Scheme for an Open-End Winding Induction Motor Drive with a Single DC Power Supply and Improved DC Bus Utilization. *IEEE Proceeding-Electric Power Applications*, 151(2), pp. 230–238. doi: 10.1049/ip-epa:20040023

Supratik, B., Debranjan, M., Suman, M. and Chandan, C. (2021). Grid-Tied Neutral Point Clamped Based Centralised Photovoltaic Inverter With Improved DC Link Voltage Balancing and Harmonic Minimisation Control. *Power Electronics and Drives*, 6(41), pp. 185–203. doi: 10.2478/pead-2021-0011

Xiaogang, W., Yongtian, Z., Ru, Y., Wei, H. and Tao, Z. (2024). Model Predictive-Based Fault-Tolerant and Power Balancing Control for Cascaded H-Bridge Inverter. *IEEE Transaction on Power Electronics*, 39(5), pp. 5257–5270. doi: 10.1109/TPEL.2023.3349311

Zhi, C., You, Z., Feifan, G. and Christopher, H. T. L. (2025). Improved Modulation for Three-Phase Series-End Winding Voltage-Source Inverters. *IEEE Transaction on Industrial Electronics*, 72(5), pp. 4546–4555. doi: 10.1109/TIE.2024.3468732